MERGING-EMERGING SYSTEMS CAN DESCRIBE SPATIO-TEMPORAL PATTERNING IN A CHEMOTAXIS MODEL

Thomas Hillen

Centre for Mathematical Biology
Department of Mathematical and Statistical Sciences
University of Alberta, Edmonton T6G2G1, Canada

Jeffrey Zielinski

Centre for Mathematical Biology
Department of Mathematical and Statistical Sciences
University of Alberta, Edmonton T6G2G1, Canada

Kevin J. Painter

Department of Mathematics and Maxwell Institute for Mathematical Sciences
School of Mathematical and Computer Sciences
Heriot-Watt University, Edinburgh, EH14 4AS, UK

(Communicated by the associate editor name)

Abstract. In a recent study (K.J. Painter and T. Hillen, Spatio-temporal chaos in a chemotaxis model, Physica D, 240 (4), 363-375, 2011) a model for chemotaxis incorporating logistic growth was investigated for its pattern formation properties. In particular, a variety of complex spatio-temporal patterning was found, including stationary, periodic and chaotic. Complicated dynamics appear to arise through a sequence of "merging and emerging" events: the merging of two neighbouring aggregates or the emergence of a new aggregate in an open space. In this paper we focus on a time-discrete dynamical system motivated by these dynamics, which we call the merging-emerging system (MES). We introduce this new class of set-valued dynamical systems and analyse its capacity to generate similar "pattern formation" dynamics. The MES shows remarkably close correspondence with patterning in the logistic chemotaxis model, strengthening our assertion that the characteristic length scales of merging and emerging are responsible for the observed dynamics. Furthermore, the MES describes a novel class of pattern-forming discrete dynamical systems worthy of study in its own right.

1. **Introduction.** The analysis of pattern formation in chemotactic systems is in full swing. Chemotaxis describes the active orientation of cells or organisms in response to chemical gradients which, in many instances, are generated and/or manipulated by the cells themselves: particular examples include soil-dwelling cellular slime molds such as *Dictyostelium discoideum* [6, 19, 9], or bacteria populations
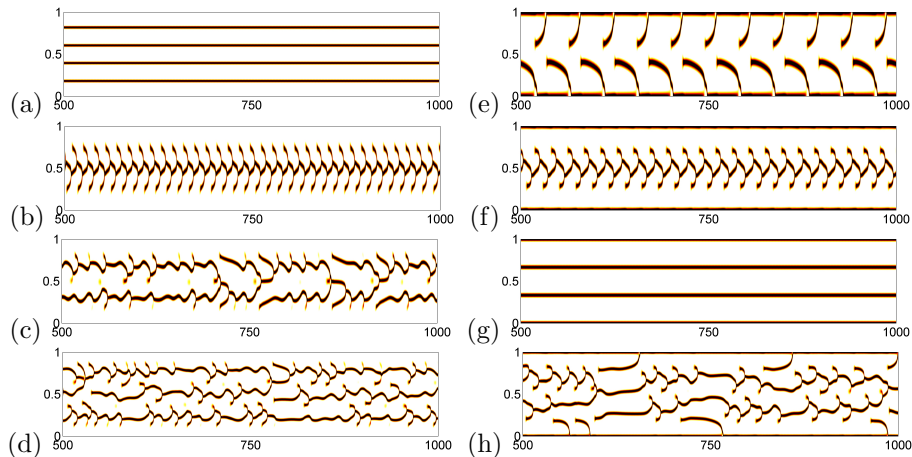
FIGURE 1. Simulations of the chemotaxis model (2) under distinct parameters and boundary conditions. Cell densities (dark indicates high densities) plotted as a function of space (y-axis) and time (x-axis). We observe stationary, periodic and chaotic patterns. (a)-(d) homogeneous Dirichlet boundary conditions, (e)-(f) homogeneous Neumann boundary conditions. Parameters are $D = r = 1$, $\chi = 10$ and (a) $L = 10$, (b) $L = 14$, (c) $L = 17$, (d) $L = 21$, (e) $L = 10$, (f) $L = 13$, (g) $L = 17$, (h) $L = 24$. Numerical method as described in text; see supplementary data for code.

such as *Eschirichia coli* [7, 20] and *Salmonella typhimurium* [26]. Here, chemotaxis and chemical signalling operate in a positive feedback loop that allows a dispersed population to self-organise into localised aggregations or swarms.

Mathematical models of this process date to the work of Keller-Segel in the early 1970s [15, 16], who developed a coupled system of nonlinear partial differential equations (PDEs) to describe the interactions between cells/organisms and their chemoattractant. This model has proved surprisingly rich, generating instabilities, pattern formation, travelling waves and finite-time blow-up amongst other properties (see the comprehensive reviews in [12, 10]). In [22] the authors studied a specific form of chemotaxis model incorporating logistic cell growth, revealing spatio-temporal dynamics ranging from stationary patterns to periodic solutions and chaotic behaviour. Notably, this complex spatio-temporal patterning phenomenon has also been reported in cultured *Eschirichia coli* populations, for example see [24, 5]. Examples of these various patterns are demonstrated in Figure 1; details of the chemotaxis model itself will be provided in Section 1.1.

Inspecting the third simulation, Figure 1 (c), we find two principal processes in operation: if two local maxima are close together, they join (*merging*), while if two local maxima are sufficiently far apart, a new maximum forms in the space between (*emerging*). These same processes apply in Figure 1 (b, d, e, f, h), although in some instances they conspire to generate a time-periodic solution. A detailed analytical understanding of these behaviours is challenging – PDE chemotaxis models generally remain intractable – and multiple lines of attack are necessary. One method,
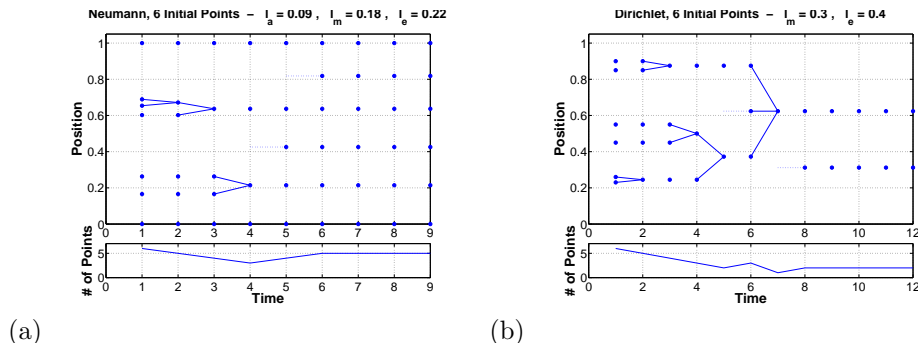
Figure 2. Illustration of the transition rules of the MES system. The top figures show the iteration step on the x-axis and the points on the interval $[0, 1]$ on the y-axis. Solid lines indicate merging events and dotted lines show emerging. The bottom figures give a count of total number of points at a given iteration step.

taken in [17], would be to carefully examine the underlying instabilities and use asymptotic methods to uncover the bifurcations.

Here we adopt a more global approach: our inspection suggested that the dynamics are determined by two principal length scales, corresponding to merging and emerging, and a principal aim is to test this assertion. To this end we explore a caricature model: a discrete analogue of the patterning process in which the numbers and positions of points on an interval are updated at each time step according to their distribution. Briefly, two points sufficiently close are merged into a single point at their midpoint (merging), while for two points sufficiently far apart a new point is inserted in the space between (emerging).

While these rules are easily explained, careful assembly is required to lay out the formal dynamical system within a suitable phase space: the *merging-emerging system (MES)*. We define this in Section 2, however previews of its output are provided in Figure 2 and 3 and selected to correlate with the PDE simulations in Figure 1. To aid presentation, merging events are illustrated through solid lines and emerging events are presaged with a dotted line leading to the new point. The lower graph tracks the number of points at each (time) step. In Figure 2 (b) we note a three-point merger at time 6; this special case, along with other "mega-mergers", is described in detail later. Figure 3 shows a case corresponding to the periodic case (b) of Figure 1, while a highly irregular case is shown in Figure 3 (b).

The manuscript is organised as follows. The remainder of the introduction recalls the logistic chemotaxis model. Section 2 is devoted to a systematic definition of the MES as a discrete set-valued dynamical system on a phase space $\mathcal{P}$. We define addition, subtraction, multiplication and a metric on $\mathcal{P}$. In Section 3 we demonstrate basic properties of the MES, including conditions for the existence of steady states, the idea of a generating set, and representations as discontinuous Poincaré maps. Section 4 illustrates the close resemblance between the patterns of the full chemotaxis PDE and those of the corresponding MES system. We also study the dependence on model parameters, the appearance of "hiccups" and the effect of stochasticity. In Section 5 we perform a statistical analysis based on multiple runs of the algorithm. The dynamical properties of the MES are shown to be far richer
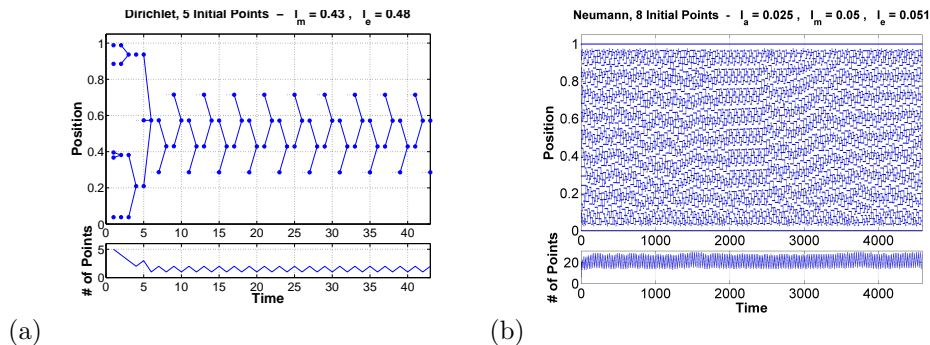
(a)   (b)

FIGURE 3. Output from MES. (a) Emerging-merging dynamics corresponding to the simple periodic chemotaxis pattern of Figure 1 (b). (b) A highly irregular example generated for small merging and emerging lengths.

than initially expected, including "hidden" periodic solutions. Yet the deterministic MES model does not appear to show chaotic dynamics, rather each simulation eventually runs into either a fixed pattern or periodic orbit (of potentially very long periods). We end with a brief discussion.

1.1. **The chemotaxis model.** The chemotaxis model considered in [22] is a coupled system of two reaction-advection-diffusion equations for the cell density $u(x,t)$ and the concentration of the chemical substance $v(x,t)$. In rescaled form, these equations are given by

$$\begin{array}{rcl} u_t &=& (Du_x - \chi uv_x)_x + ru(1-u)\,, \\ v_t &=& v_{xx} + u - v\,. \end{array} \tag{1}$$

In the above $x \in [0, L], L > 0$ denotes space, $t \geq 0$ is time, r relates to a population growth rate and D and χ are a scaled diffusion coefficient and chemotactic sensitivity, respectively. The index notation denotes partial derivatives. For the current paper it is convenient to further rescale onto the unit domain $[0, 1]$: setting $\tilde{x} = x/L$,

$$\begin{array}{rcl} u_t &=& (\frac{D}{L^2}u_x - \frac{\chi}{L^2}uv_x)_x + ru(1-u)\,, \\ v_t &=& \frac{1}{L^2}v_{xx} + u - v\,, \end{array} \tag{2}$$

where we have subsequently dropped the tildes for notational convenience. Model (2) is typically equipped with one of three standard boundary conditions:
(a) homogeneous Neumann boundary conditions,

$$u_x(0,t) = u_x(1,t) = v_x(0,t) = v_x(1,t) = 0\,;$$

(b) homogeneous Dirichlet boundary conditions,

$$u(0,t) = u(1,t) = v(0,t) = v(1,t) = 0\,;$$

(c) periodic boundary conditions,

$$\begin{array}{rcl} u(0,t) = u(1,t), && v(0,t) = v(1,t), \\ u_x(0,t) = u_x(1,t), && v_x(0,t) = v_x(1,t). \end{array}$$

Model (2) with any of the above boundary conditions possesses rich dynamical behaviour, including stationary patterns, periodic solutions and chaotic dynamics:

see Figure 1. Note that the simulations of (2) have been performed using the Matlab internal PDE solver (pdepe); the numerical code is available for download in the supplementary data (or at request from the authors). Simulations have been further tested and compared against "home-grown" codes (see numerical methods in [22]): the distinct methods produce equivalent output, although a precise quantitative match across the full parameter space is precluded due to the chaotic properties/sensitive dependence in the PDE system. Further examples are shown throughout this paper, along with [22, 25, 2, 11] and references therein.

In [22] an estimate for the emerging length was obtained via a critical domain-size problem. In the rescaled model (2) the emerging length is

$$l_e = 2\pi \sqrt{\frac{D}{L^2 r}}.$$

Note that for the examples presented, where $D = r = 1$, $\chi = 10$, this simplifies to

$$l_e = \frac{2\pi}{L}. \tag{3}$$

2. **Merging emerging systems.** In this section we formulate a caricature discrete dynamical system of the merging-emerging dynamics. We note that under Dirichlet boundary conditions the chemotaxis PDE model (2) only generates interior aggregates (e.g. see Figure 1 (a-d)), while under Neumann boundary conditions two local maxima typically form at the boundaries $x = 0$ and $x = 1$ and remain fixed throughout (e.g. see Figure 1 (e-h)). Either way, we are fundamentally interested in the dynamics of interior points on the unit interval $[0, 1]$. Prior to the definition of the MES, we consider the phase space.

2.1. **Phase Space.**

Definition 2.1. A <u>finite partition of unity</u> (or "partition", for short) is a finite subset of $[0, 1]$ that contains 0 and 1. Let $\mathcal{P}$ denote the set of all finite partitions of unity.

Obviously, $\mathcal{P}$ is not empty and we denote $e := \{0, 1\} \in \mathcal{P}$. A finite partition of unity $\{a_j\}$ can always be arranged as

$$0 = a_0 < a_1 < \cdots < a_n = 1.$$

We define three operations on P: addition $(+)$, subtraction $(-)$ and multiplication $(\cdot)$. P is closed with these operations and they carry several algebraic properties.

Definition 2.2. Given $a, b \in \mathcal{P}$, $a = \{a_0, \ldots, a_n\}, b = \{b_0, \ldots, b_k\}$.

1. We define addition, $+$, by

$$a + b := a \cup b.$$

2. Let $\tilde{a} \subset a$. Then we define subtraction, $-$, by

$$a - \tilde{a} := a \backslash \tilde{a} + \{0, 1\}.$$

3. We define multiplication, $\cdot$, by

$$a \cdot b := \{a_0 b_0, a_1 b_0, \ldots, a_n b_0, a_0 b_1, \ldots, a_n b_1, \ldots, a_n b_k\}.$$

Addition, subtraction and multiplication have the following properties.

- $\mathcal{P}$ is closed with respect to (w.r.t.) addition. Addition has a neutral element $e = \{0, 1\}$ such that $a + e = a$. Each element is idempotent, $a + a = a$. Addition is commutative, $a + b = b + a$, and associative, $a + (b + c) = (a + b) + c$, for $a, b, c \in \mathcal{P}$.
- Note that subtraction is normally defined through solvability of the equation $a + x = b$. Here, however, this equation is generally not solvable in $\mathcal{P}$. Hence our subtraction is not the inverse operation of addition. However, we do have the following relations:
$$(a + b) - b = a\,;$$
for $\tilde{a} \subset a$,
$$(a - \tilde{a}) + \tilde{a} = a\,;$$
and there is the inverse element
$$a - a = e\,.$$
Note, however, that $-a \notin \mathcal{P}$, and hence the inverse element is not in the set.
- $\mathcal{P}$ is closed w.r.t. multiplication, since $a_0 b_0 = 0$ and $a_n b_k = 1$. Multiplication is commutative, i.e. $a \cdot b = b \cdot a$, and it has a neutral element e, i.e. $a \cdot e = a$. The neutral element e is neutral for both addition and multiplication; hence, P is not an algebra. It is, however, a monoid with respect to addition.
- $+$ and $\cdot$ satisfy the distributive law, i.e.
$$(a + b) \cdot c = a \cdot c + b \cdot c.$$
- Partitions can be multiplied by a scalar $\mu \in [0, 1]$ in the following way
$$\mu a := \{\mu a_0, \mu a_1, \ldots, \mu a_k\} \cup \{1\}.$$
Using this multiplication, we have the relations
$$\mu(a + b) = \mu a + \mu b$$
and
$$\mu(a \cdot b) = \mu a \cdot b = a \cdot \mu b.$$

2.2. **Metric on $\mathcal{P}$.** We can introduce topologies on $\mathcal{P}$ by using mollifier functions. For $0 < h < 1$ and $0 \leq a_j \leq 1$ we define
$$\phi(x) := \exp\left(-\left(\frac{x}{h}\right)^2\right), \qquad \psi(x; a_j) := \frac{\phi(x - a_j)}{\int_0^1 \phi(x - a_j)dx},$$
such that
$$\int_0^1 \psi(x, a_j)dx = 1.$$
For $a = \{a_0, \ldots, a_n\} \in P$ we define an <u>indicator function</u> of a by summing over all internal points (excluding 0 and 1):
$$\Psi(x; a) := \sum_{j=1}^{n-1} \psi(x; a_j)\,.$$
Then
$$N(a) := \int_0^1 \Psi(x; a)dx$$
is the number of internal points of a. For the neutral element e we have $N(e) = 0$.

We define two distance measures on P as follows:

$$d_1(a,b) := \int_0^1 |\Psi(x;a) - \Psi(x;b)| dx \,,$$

$$d_2(a,b) := \left(\int_0^1 |\Psi(x;a) - \Psi(x;b)|^2 dx \right)^{1/2} .$$

The above, of course, mimic the L^1 and L^2 distances.

Properties of the distance functions are as follows:

- clearly, $d_1 \geq 0, d_2 \geq 0$, $d_1(a,b) = d_1(b,a)$ and $d_2(a,b) = d_2(b,a)$;
- we have
$$d_1(a,b) = 0 \quad \Leftrightarrow \quad d_2(a,b) = 0 \quad \Leftrightarrow \quad a = b \,;$$
- based on the properties of the L^1 and L^2 norms, for $a, b, c \in \mathcal{P}$ we have the triangle inequality,
$$d_j(a,b) \leq d_j(a,c) + d_j(b,c), \qquad j = 1, 2 \,;$$
- we note $N(a) = d_1(a,e)$. If $|a|$ denotes the size of the set a, then $|a| = N(a)+2$.
- $N(a) \geq 0$ and $N(a) = 0$ iff $a = e$;
- arbitrary sets $a, b \in \mathcal{P}$ may have common points, hence
$$N(a+b) \leq N(a) + N(b) \,;$$
- for any $\mu \in (0,1)$ we have
$$N(\mu a) = N(a) + 1 \,.$$

Hence, d_1 and d_2 define a metric on $\mathcal{P}$ and $\mathcal{P}$ is a metric set with addition, subtraction and multiplication. Unfortunately, $N(.)$ is not a norm since it is not homogeneous of order one.

2.3. **Merging and emerging dynamics.** We are now in a position to define a time-discrete dynamical system on $\mathcal{P}$. We consider two non-negative model parameters l_m and l_e, respectively termed the merging length and the emerging length. The definition of the MES system requires attention to a number of special cases, which we consider in an incremental manner. Here we only define the base-case, which we call (E_0, M_0), where E_0 describes an emerging operator and M_0 a merging operator. While the base case ignores some more complicated scenarios, it helps introduce the notation; in the Appendix a systematic specialisation is taken towards the final model $(\hat{E}_2, \hat{M}_1)$, closest in description to the behaviour observed in PDE simulations. As in the PDE case, we distinguish between Neumann and Dirichlet boundary conditions. For the Neumann-case we impose fixed local maxima at the boundaries with nearby points absorbed into these, whereas for the Dirichlet case there are generally no boundary points. The emerging operator is the same for each boundary condition, but the merging operator in the Neumann case must incorporate absorption to the boundary. Absorption is described by an additional absorption length parameter, l_a, usually taken as $l_a = l_m/2$.

Base case:

- **Emerging:** *Given $a \in \mathcal{P}$ and an emerging length $l_e > 0$. We combine all intervals with a length larger than l_e in an emerging index set* $J_e^0 := \{j : |a_{j+1} - a_j| > l_e\}$. *The emerging operator $E_0 : \mathcal{P} \to \mathcal{P}$ is defined as*
$$E_0(a) := a + \sum_{J_e^0} \left\{ \frac{a_{j+1} + a_j}{2} \right\} .$$

- **Merging, Neumann:** *Given $a \in \mathcal{P}$ and a merging length $l_m > 0$.* Inner intervals that have a length smaller than l_m will merge. At the boundary, merging to the boundary (*absorption*) occurs if the distance is less than $l_a = l_m/2$. Hence, here we define two *merging index sets*: $J_m^0 := \{j : |a_{j+1} - a_j| < l_m, j = 2, \ldots, n-1\}$; $\tilde{J}_m^0 := \{1 : a_1 < l_m/2\} \cup \{n-1 : 1 - a_{n-1} < l_m/2\}$. Then the *merging operator* $M_0 : \mathcal{P} \to \mathcal{P}$ is defined as

$$M_0(a) := a - \sum_{\tilde{J}_m^0} \{a_j\} - \sum_{J_m^0} \{a_{j+1}, a_j\} + \sum_{J_m^0} \left\{ \frac{a_{j+1} + a_j}{2} \right\}.$$

- **Merging, Dirichlet:** In the Dirichlet case we no longer assume to have $a_0 = 0$ and $a_n = 1$ and the phase space in this case is $\mathcal{P}_D := \{$finite subsets of $(0, 1)\}$. *Given $a \in \mathcal{P}_D$ and a merging length $l_m > 0$.* Intervals that have a length smaller than l_m will merge. We define a *merging index set*: $J_m^0 := \{j : |a_{j+1} - a_j| < l_m, j = 2, \ldots, n-1\}$. Then the *merging operator* $M_0 : \mathcal{P}_D \to \mathcal{P}_D$ is defined as

$$M_0(a) := a - \sum_{J_m^0} \{a_{j+1}, a_j\} + \sum_{J_m^0} \left\{ \frac{a_{j+1} + a_j}{2} \right\}.$$

- The merging-emerging system (MES) is then defined by the iteration map $A_0 : \mathcal{P} \to \mathcal{P}$ with $A_0 := E_0 \circ M_0$ (or $\tilde{A}_0 := M_0 \circ E_0$) in the Neumann case or $A_0 : \mathcal{P}_D \to \mathcal{P}_D$ in the Dirichlet case.

Note that any of the above index sets J can be empty in a given situation. The above model defines the *base model*, incorporating the simplest dynamics. We also consider more advanced rules that deal with special cases that might arise. For example, two merging intervals of the same interval length might occur side-by-side: the PDE model in this instance shows the quasi-simultaneous merging of three aggregates into one, which we call a *mega-merger* (*cf.* Figure 1 (c) at time 850, or (d) at around 770). Further, if two merging intervals of different length occur, then the shorter one would merge first. Including these more realistic rules requires advanced merging and emerging operators: we refer to Figure 17 for a schematic and Appendix A for precise details.

It is possible to compute some explicit example by hand. For example, assuming the Dirichlet base case we find:

- Example 1: $l_m = 0.5 + \epsilon, l_e = 0.5 - \epsilon$,

$$\{1/2\} \xrightarrow{E} \{1/4, 1/2, 3/4\} \xrightarrow{M} \{3/8, 5/8\} \xrightarrow{E} \{3/8, 5/8\} \xrightarrow{M} \{1/2\} \xrightarrow{E} \ldots$$

- Example 2: $l_m = 0.5 - \epsilon, l_e = 0.5 + \epsilon$,

$$\{1/2\} \xrightarrow{E} \{1/2\} \xrightarrow{M} \{1/2\} \xrightarrow{E} \ldots$$

- Example 3: $l_m = 0.5 - \epsilon, l_e = 0.5 + \epsilon$,

$$\{4/7\} \xrightarrow{E} \{2/7, 4/7\} \xrightarrow{M} \{3/7\} \xrightarrow{E} \{3/7, 5/7\} \xrightarrow{M} \{4/7\} \xrightarrow{E} \ldots$$

Examples 1 and 2 illustrate how a subtle change in the emerging and merging lengths can lead to distinct dynamics (periodic or stationary) from the same initial state; Examples 2 and 3 illustrate how distinct initial conditions can generate distinct dynamics for identical emerging and merging length parameters.

3. **Some basic properties of the MES.** To identify some basic properties we consider $A_0 = E_0 \circ M_0$, where E_0 and M_0 are given by the base case for Neumann boundary conditions. We expect that similar properties hold for more advanced cases, but it exceeds the present aims to go through all cases in detail.

3.1. **Steady States.** A general steady state $\bar{a}$ satisfies $\bar{a} = A\bar{a}$. This can arise in two ways: (i) *trivial steady states*, which satisfy $\bar{a} = M\bar{a}$ and $\bar{a} = E\bar{a}$; (ii) *merging-emerging (me) steady states*, which satisfy $\bar{a} = A\bar{a}$ but $\bar{a} \neq M\bar{a}$, hence only a combination of merging and emerging leads to a steady state.

Lemma 3.1. *Let $l_e \geq l_m > 0$ and consider the MES in the base case with Neumann boundary conditions.*

1. *A (trivial) steady state $\bar{a}$ of size $n + 1 = |\bar{a}|$ only exists if*

$$\frac{1}{l_e} \leq n \leq \frac{1}{l_m} + 1. \tag{4}$$

   If no integer exists satisfying (4), there is no steady state.
2. *me-steady states can only result from absorption at the boundary. They do not exist for the Dirichlet case.*

Proof. We study trivial steady states first. The condition $\bar{a} = M\bar{a}$ requires that no merging occurs, which translates into three conditions:

$$a_1 \geq \frac{l_m}{2}, \quad 1 - a_{n-1} \geq \frac{l_m}{2}, \quad |a_{j+1} - a_j| \geq l_m, \forall j = 2, \ldots, n-1.$$

This already defines a maximum of interior points that a trivial steady state can support. If $n + 1 = |\bar{a}|$ and $\bar{a} = \{a_0, \ldots, a_n\}$ then, from the above inequalities, it follows that

$$\begin{aligned}
1 &= a_1 + \sum_{j=1}^{n-2} |a_{j+1} - a_j| + 1 - a_{n-1}, \\
&\geq \frac{l_m}{2} + (n-2)l_m + \frac{l_m}{2}, \\
&= (n-1)l_m.
\end{aligned}$$

This leads to the condition

$$\frac{1}{l_m} + 1 \geq n.$$

Hence, given l_m, the MES can only support steady states which have at most $1/l_m + 1$ points.

In the case of emerging, the condition $\bar{a} = E\bar{a}$ requires that all intervals are shorter than or equal to l_e, i.e.

$$|a_{j+1} - a_j| \leq l_e \quad \text{for all } j = 1, \ldots, n.$$

Then

$$1 = \sum_{j=1}^{n} |a_{j+1} - a_j| \leq nl_e$$

gives a minimum number of points of $n \geq \frac{1}{l_e}$.

To obtain me-steady states which are not trivial steady states, we require $\bar{a} \neq M\bar{a}$. Hence at least one merging event must occur. This merging event can arise

in the interior or at one of the boundaries. An interior merging event gives an additional point $\hat{a} := (a_{j+1} + a_j)/2$ for some j, however $\hat{a} \notin a$. If we now apply E then we can never remove this additional point and $E \circ M\bar{a} \neq \bar{a}$. Hence inner merging events cannot occur.

If merging occurs at one of the boundaries, the point is absorbed into the boundary. If then $a_1 > l_e$ or $1 - a_{n-1} > l_e$, this point could be replaced through an emerging event.

$\square$

3.2. **Generating set.** Due to the fundamental root of the dynamics in terms of retaining points and taking pairwise mean values, we can consider a restriction of the set of partitions $\mathcal{P}$ to be rational numbers

$$\mathcal{P}_Q := \{\{a_0, \ldots a_n\}; a_0 = 0, a_n = 1, a_j < a_{j+1}, a_j \in \mathbb{Q}; \ j = 1 \ldots n - 1\}$$

where $\mathcal{P}_Q$ is closed w.r.t. the MES system.

Moreover, the initial set of points can be viewed as a generating set for the dynamics in the following sense. Given an initial value $a = \{a_0, \ldots a_n\} \in \mathcal{P}$, then, in each iteration step, we can add at most the mean value of two neighbouring points. We define the following elements of $\mathcal{P}$ as

$$S_a^0 := a, \qquad S_a^1 = a + \sum_{j=1}^{n} \left\{ \frac{a_j + a_{j-1}}{2} \right\},$$

and, given $S_a^{k-1} = \{s_0^{k-1}, \ldots, s_N^{k-1}\}$, we define recursively

$$S_a^k := S_a^{k-1} + \sum_{j=1}^{N} \left\{ \frac{s_j^{n-1} + s_{j-1}^{n-1}}{2} \right\}.$$

In the limit, we define

$$S_a := \bigcup_{k=0}^{\infty} S_a^k.$$

Lemma 3.2.   *1. For each finite time k, the dynamics of the MES is contained in the finite set S_a^k.*
    2. For each initial condition $a \in \mathcal{P}$ the set S_a is dense in $[0, 1]$.

Proof. Statement 1 is obvious, hence we only need to prove 2. Consider $x \in [0, 1]$ with $x \notin \bigcup_{k=0}^{\infty} S_a^k$. For each $k > 0$ there exists an interval $(s_{j_k}^k, s_{j_k+1}^k)$ of elements in S_a^k that contains x. The length of this interval is bounded by

$$|s_{j_k+1}^k - s_{j_k}^k| \le \frac{1}{2^k},$$

which converges to 0 as $k \to \infty$.

$\square$

Although the first statement of Lemma 3.2 offers hope of dealing with a finite set of possible points, the second statement shows that the dynamics are not a priori restricted and can in fact involve the whole interval $[0, 1]$.
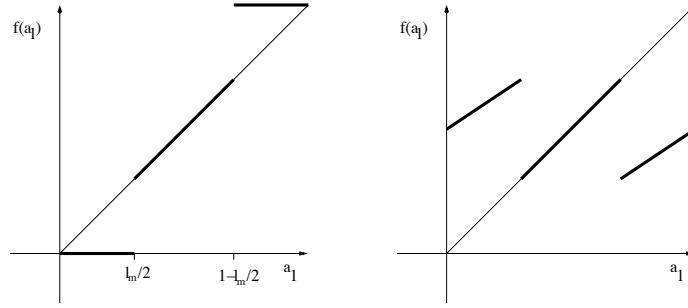
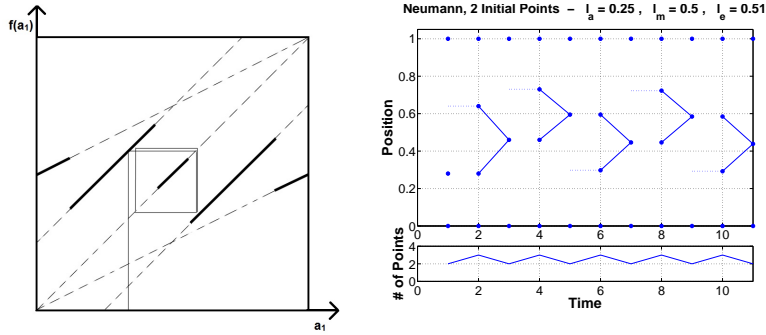FIGURE 4. Poincare's maps for case 1 (left) and case 2 (right); see text for details.

FIGURE 5. Poincare's maps for case 3 (left) and the corresponding MES simulation (right).

3.3. **Relation to discontinuous Poincaré maps.** Some simple cases can be directly related to discontinuous Poincaré maps, indicating the type of dynamical system to be expected. To see this, we consider a special case where, after each iteration with A, we have exactly one internal point. We can then define a map which maps the internal point to its image: if $a := \{0, a_1, 1\}$, then

$$f(a_1) := (A(a))_1.$$

This can then be plotted as an iterative map (cobweb).

Case 1. Assume $l_e > 1 > 2l_m$. Emerging never occurs and merging can only happen if the inner point is sufficiently close to the boundary. The map f for this case is illustrated as the thick line in the left graph of Figure 4.

Case 2. Assume $l_e <\approx 1$ and $l_m \ll 1$: if the inner point is close to a boundary we have one emerging and one merging event, while if it is close to the centre nothing occurs. For this case the Poincaré map is shown in the right graph of Figure 4.

Case 3. If we make the emerging length in Case 2 smaller, then we can expect periodic behaviour. In Figure 5 we show the Poincaré map for the case $0.5 < l_e < 1, l_m \approx 0.5$, where cobwebbing reveals a periodic orbit. The corresponding MES simulation is shown in the right plot of Figure 5.
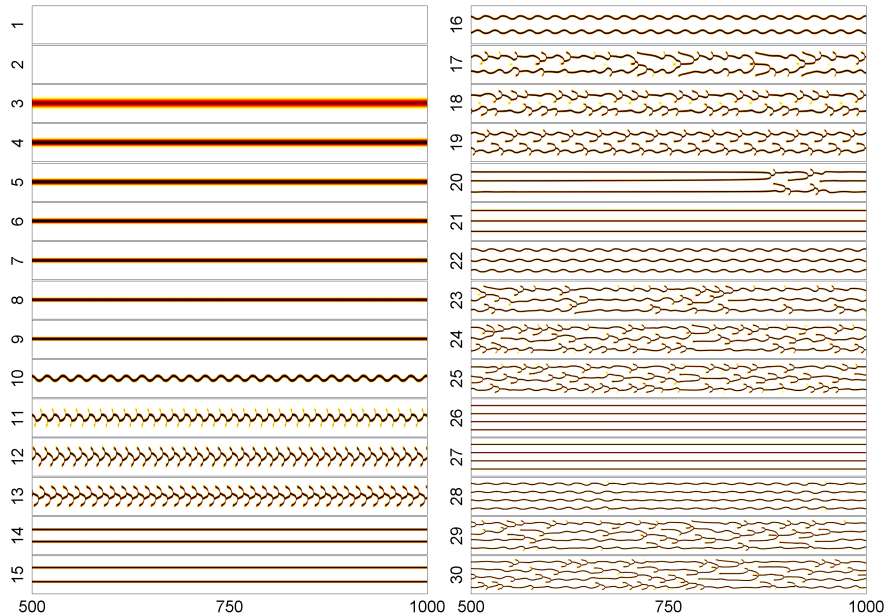
FIGURE 6. PDE simulations of the Dirichlet problem (2) under varying L (as indicated to the left of each plot). Simulation details and other parameters as in Figure 1.

It is known that discontinuous Poincaré maps can generate complicated patterns, including chaotic dynamics [14]. The MES show features of these discontinuous systems.

4. Discrete patterns.

4.1. **Comparison to the chemotaxis PDE.** In this section we compare "pattern formation" properties in the MES with those of the full chemotaxis model (2). Figure 6 shows simulations of the Dirichlet problem for (2), where L is used as a bifurcation parameter to show changes in dynamical behaviour across parameter space: for these parameters, the estimated emerging length in the chemotaxis model is $l_e = 2\pi/L$. In the following figure, Figure 7, we show iterations of the corresponding MES system $(\hat{E}_2, \hat{M}_1)$ with l_e defined from this estimate.

Notably, the essential qualitative properties of the full chemotaxis model are also contained within the MES: figures 2 and 3 have already demonstrated stationary and periodic patterns. In Figure 7 we note that steady states can emerge from periodic behavior ($L = 20$), or the dynamic remains periodic/irregular ($L = 18, 25, 29$). Note that for $L = 25$ there is a periodic structure of approximately period 50. Typically, at a given point in (l_m, l_e)-parameter space, we can observe multiple behaviours according to the initial conditions: certain initial conditions evolve to a steady state, while others lead to periodic patterns of varying period (see Figure 8). Note that distinct initial conditions also lead to distinct pattern types for the full chemotaxis model (2).
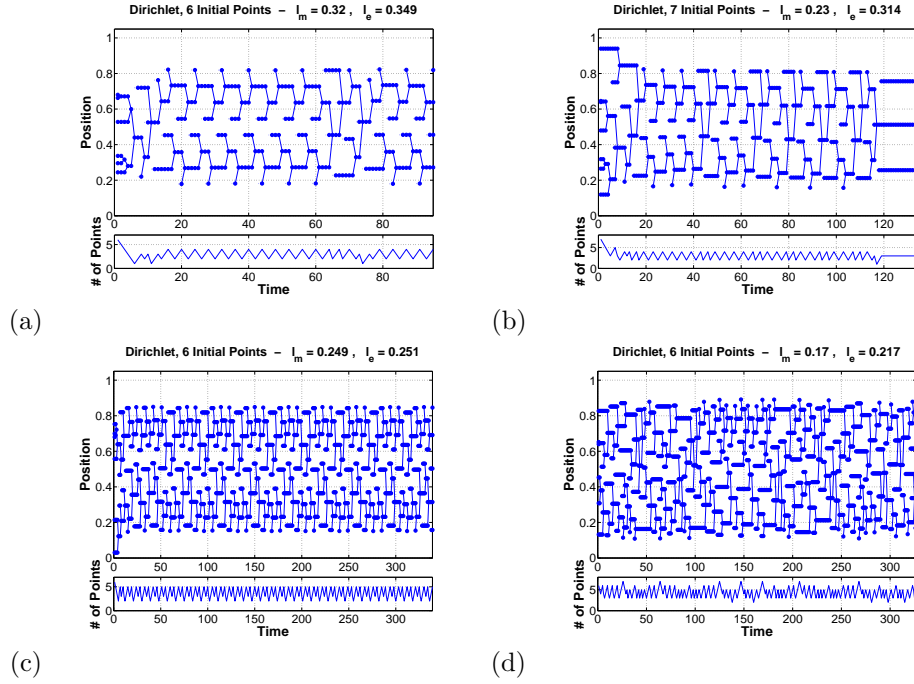
FIGURE 7. MES simulations for the Dirichlet case. We set $l_e = 2\pi/L$ for (a) $L = 18$, (b) $L = 20$, (c) $L = 25$ and (d) $L = 29$.
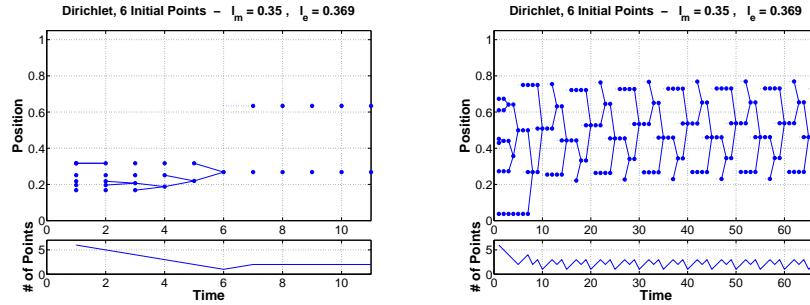

FIGURE 8. Two simulations of the MES for Dirichlet boundary conditions, employing the same parameter values but distinct initial conditions. Here we set $L = 17$.

In Figure 9 we plot simulations of the Neumann problem for (2), once again using L as the bifurcation parameter; note that we typically have maxima at the domain boundaries and hence local maxima are also imposed at the boundary of the MES system. Similar to the Dirichlet case, we obtain stationary and periodic solutions, where the period lengths vary considerably. In Figure 10 we shows two examples of an iteration that relaxes to a steady state ($L = 22$) and an example of a long and complicated period ($L = 27$). We tested many more parameter values which are
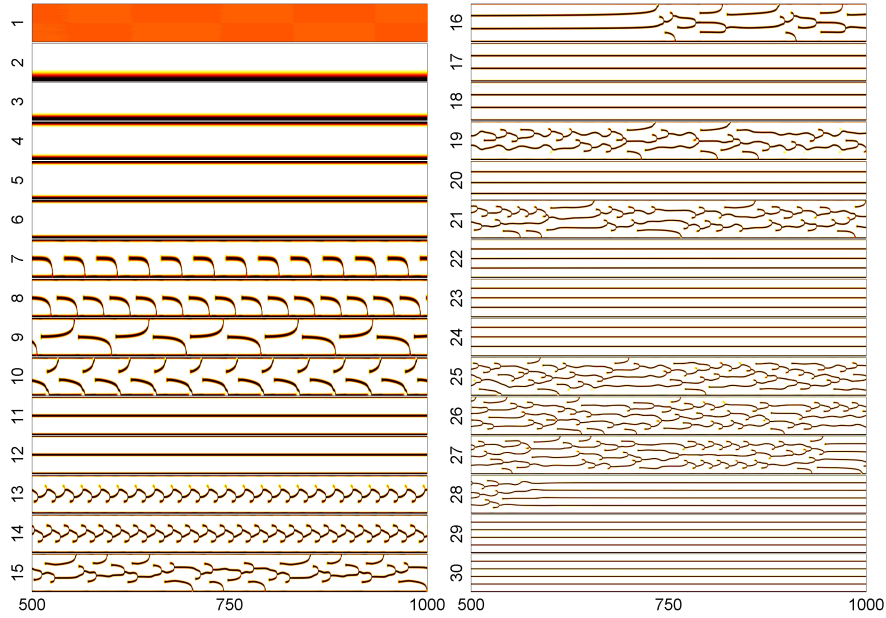
FIGURE 9. PDE simulations of the Neumann problem (2) under varying L (as indicated to the left of each plot). Simulation details and other parameters as in Figure 1.
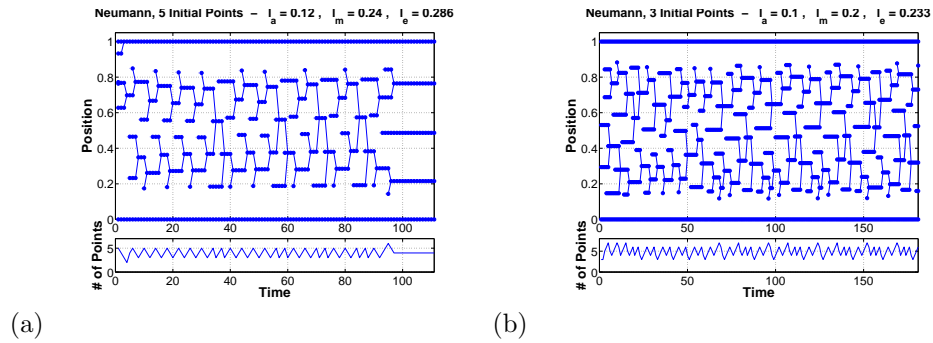

(a)   (b)

FIGURE 10. MES simulations for the Neumann case. We set $l_e = 2\pi/L$ for (a) $L = 22$ and (b) $L = 27$.

not shown here and we again observe close resemblance between the full chemotaxis model and the MES.

4.2. **Base case.** Notably the base case (E_0, M_0) does not reveal this rich behaviour: simulations indicate that the dynamics either evolve to a steady state or a periodic orbit with a rather short period (two or three time steps). Simulations in Figure 11 show two simulations of the base case under Neumann boundary conditions. Dynamics appear to be dominated by an oscillation of small period, disturbed from time to time through interaction with the boundary as the system attempts to reach a "comfortable" arrangement with quasi-equal spacing. Qualitative differences arise
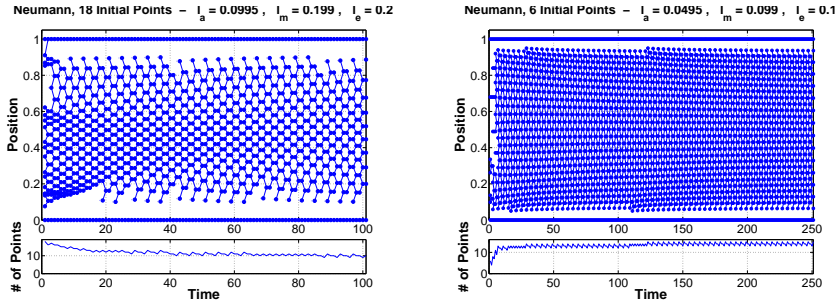
FIGURE 11. Two base case simulations under Neumann boundary conditions for $l_m = 0.199, l_e = 0.2$ (left) and $l_m = 0.099, l_e = 0.1$ (right).
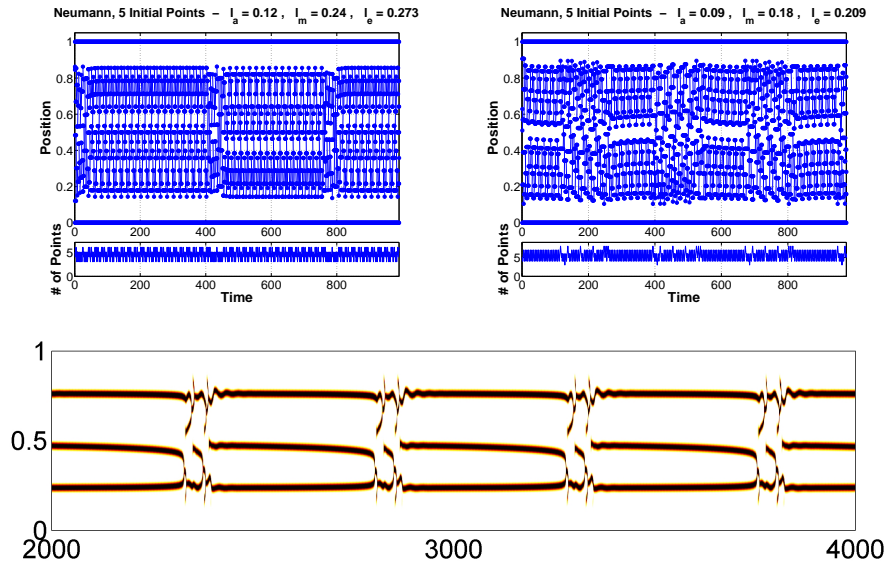

FIGURE 12. "Hiccup"-simulations for the MES Neumann case with $L = 23$ (left) and $L = 30$ (right). Similar phenomena occur in the PDE model, shown for Dirichlet case and $L = 20$.

according to whether dynamics fan outwards (e.g. left figure) as the system slowly loses points, or fan inwards (e.g. right figure) as the system tries to gain points.

4.3. **Hiccups.** A number of simulations reveal "hiccups": seemingly ordered structure interspersed with bursts of less regular behaviour. In Figure 12 (a) we show two examples of this phenomenon for $L = 23$ and $L = 30$ and Neumann boundary conditions. Interestingly, the PDE chemotaxis model (2) can display somewhat similar phenomena. Similar phenomena of intermittent bursting can be found in very different contexts, such as turbulence "puffs" in pipeline flow [4] and bursting for coupled neurons [8].
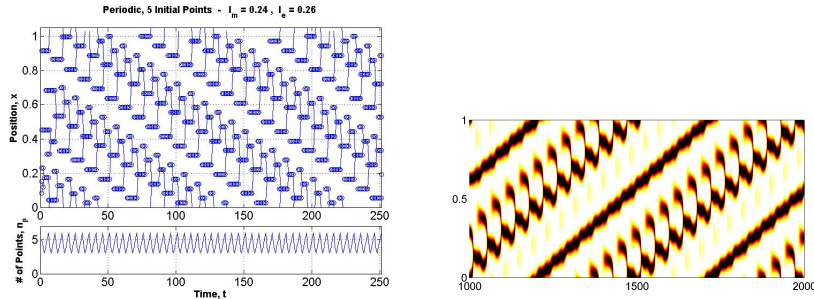
FIGURE 13. Periodic boundary conditions: Typical rotating patterns for the MES (left) and for the PDE model (right)

4.4. **Periodic boundary conditions.** It is straightforward to define the MES for periodic boundary conditions as well: here, the region is wrapped onto a circle and there is no need to define distinct rules for points closest to the "boundaries". For the periodic case a variety of solutions can again be found, including the new form of a periodic orbit that rotates as a "travelling wave" about the unit sphere, see Figure 13 (left). Notably, such solutions can also be found in the full PDE model: an example is shown in Figure 13 (right).

4.5. **Inclusion of randomness.** The "definitive" insertion/merging of points in the MES – at the exact middle of the interval – is obviously an approximation of behaviour in the PDE simulations, where precise locations of merging and emerging events vary according to the mass of individual aggregates and their distribution across the domain. This source of variability can be introduced into the MES via a small random perturbation. Specifically, if x_1, x_2 denote two points that either merge or admit an emerging event, then we define the new "middle" location as

$$x_{\text{new}} = x_1 + (x_2 - x_1)(0.5 + \text{random}\{-1, 1\}(x_2 - x_1)10^{-5}).$$

Here we no longer require a mega-merger rule, since equal intervals do not arise (unless present in the initial condition). Simulations of $(\hat{E}_2, \hat{M}_1)$ with this random offsetting are shown in Figure 14. We note a more irregular structure than in previous simulations, with no clear periodic structure and more in line with the seemingly chaotic patterning in the deterministic PDE. This indicates that the deterministic MES system describes some of the dynamics of the PDE chemotaxis system, but not all. It seems that a random component is also relevant. In this case the MES becomes a stochastic set-valued dynamical system, which we will not analyse further in this manuscript.

5. **Statistical Analysis.** A PDE model such as (2) is encumbered by its computational demand, limiting studies to localised investigations rather than exhaustive sweeps throughout parameter space. The MES model, on the other hand, is quick and simple to implement and allows highly detailed investigations with statistical analysis following repetitions under distinct initial conditions. Again, we use model $(\hat{E}_2, \hat{M}_1)$ with Dirichlet boundary conditions and focus on the parameter region

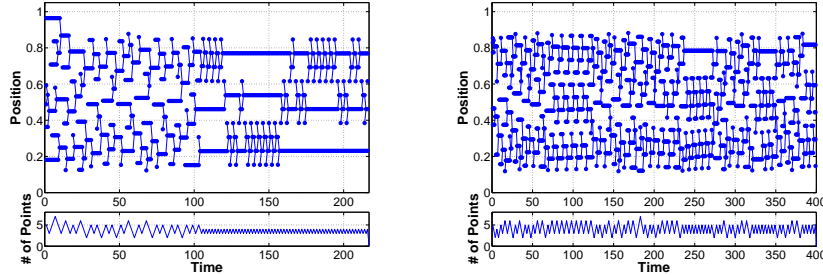$$(l_m, l_e) \in [0.23, 0.25] \times [0.25, 0.27].$$

FIGURE 14. Stochastic MES simulations for the Dirichlet case with $l_m = 0.22$ and $l_e = 0.245$ (left) and $l_e = 0.23$ (right).

The emerging length l_e corresponds to an interval length of $L = 2\pi/l_e \in [23.27, 25.13]$, an area of interesting dynamics in the PDE model: see Figures 6 and 7. We increment l_m and l_e in steps of 0.001 and, for each (l_m, l_e) pair, run 50 simulations from one, randomly chosen, initial point. The maximum run-time for each simulation is set at $n = 2000$ and we monitor the dynamics for steady states or periodic orbits. The latter are identified through a detection algorithm which compares pieces of orbits: setting a tolerance level of 10^{-15}, orbits are identified as periodic if the distance between successive periods is less than this tolerance. Note that checks for lower tolerances $(10^{-20}, 10^{-30})$ generated the same periods and the same period lengths for each parameter pair (l_m, l_e). We find that all runs become either steady states or periodic orbits, although the period can be as long as 350 iteration steps.

In Figure 15 we plot, at each parameter pair (l_m, l_e), the initial point in blue if the iteration becomes stationary and in pink if it becomes periodic. Due to the convoluted nature of the three dimensional picture, we take side-views below: on the left we show the projections onto the (l_e, IC)-plane and on the right we show the projections onto the (l_m, IC)-plane; top frames plot the initial points that become steady states (blue) while bottom frames plot the initial points that become periodic (pink). We clearly see that the resulting pattern depends considerably on l_e but less so on l_m. A complicated mixing of periodic and stationary outcomes is observed, with periodic regions interspersed with stationary "tongues". Figure 15 (top right) plots the fraction of initial conditions that evolve to fixed patterns; again, we observe the greater dependence on l_e than l_m.

We note that the period length of the periodic solutions can range from approximately 14 to 350, with a sharp transition at $l_e \approx 0.268$, see Figure 16. Standard deviations (not shown) vary from 5-6 in the region of period lengths around 16, to circa 100 for regions with periods above 300. The long period solutions are typically of hiccup type (see bottom row of Figure 16). In Figure 16 (middle row) we plot the length of time until either a periodic orbit or stationary solution (to a tolerance of 10^{-15}) is obtained. Here we also note a sharp transition about $l_e = 0.265$, in which short period solutions form following a long transient time, while long periods are found quickly. As previously we note strong dependence on l_e but weak dependence on l_m.
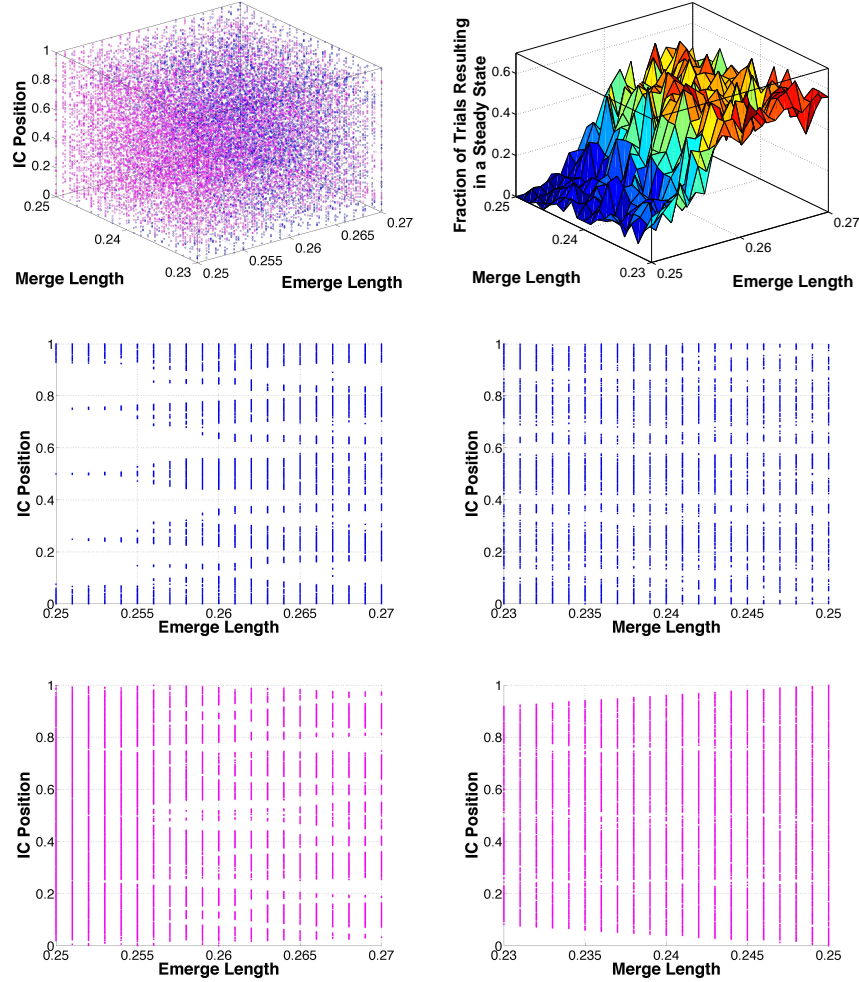
FIGURE 15. Top left: Outcome of the MES simulations with $(l_m, l_e) \in [0.23, 0.25] \times [0.25, 0.27]$. Blue points indicate initial conditions that lead to stationary solutions, while pink indicate those that lead to periodic orbits. Top right: Fraction of trials that result in a steady state as a function of (l_m, l_e). Middle and bottom row: Side views of the top left figure for initial conditions that lead to steady states (middle) or to periodic orbits (bottom). Note the symmetry about the midplane of IC=0.5 (color version online).

6. **Conclusion.** Chemotaxis models have been the subject of interest for their patterning properties. In particular the logistic chemotaxis model (1) demonstrates rich patterning, for example see [1, 25, 22, 18, 3, 11] and references therein. In [22] a systematic numerical analysis for this system was conducted, revealing stationary and spatio-temporal patterns of both time-periodic and chaotic fashion; the latter developing through the merging of neighbouring aggregates and the emergence of new aggregates in open spaces. Similar behaviour has been observed in a number of
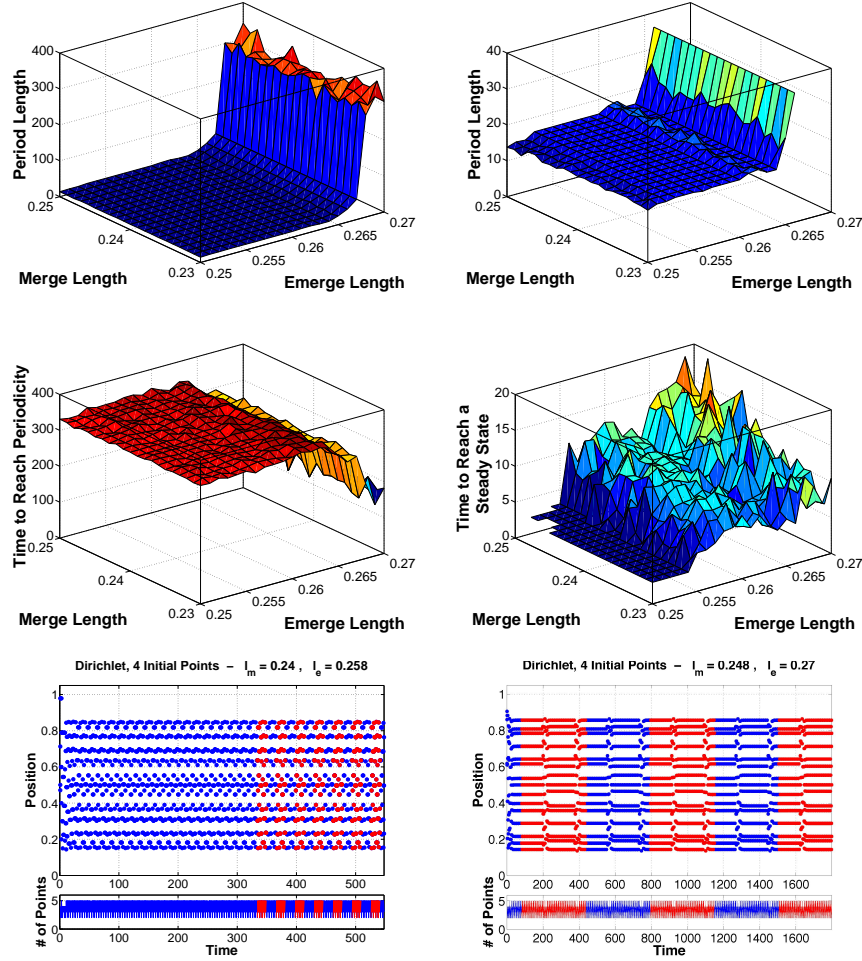
FIGURE 16. Top row: Mean period length of the orbits that be-
came periodic; left: full range, right: restricted to $l_e \leq 0.266$.
Middle row: Average time to reach periodicity (left) and stationar-
ity (right). Bottom row: two examples of periodic patterns, where
the left is of short period and the right is a long-period hiccup
pattern. Individual periods have been highlighted in red and blue
(color version online).

specific applications of models incorporating chemotaxis processes, such as models
for tumour-macrophage interactions [21], tumour invasion [2] and host-parasitoid
dynamics [23]. Furthermore, cultured *Eschirichia coli* bacteria populations can also
exhibit highly dynamic patterning, the nature of which has been shown to be well
replicated by models of the form (2): see [24, 5] for details.

In this paper we have developed a discrete dynamical system, called the merging-
emerging system (MES), to investigate the extent to which chemotaxis dynamics
are driven by the merging-emerging process. Intuitively, merging is driven through

the chemotaxis-induced attraction between neighbouring aggregates: how quickly merging can occur will depend on their closeness, and in turn on the range of chemotactic action. Emerging will also depend on the space between aggregates, and whether a new aggregate can develop through proliferation before becoming absorbed into one of its neighbours. This suggests two characteristic length scales for the merging and emerging processes, and the MES system is formulated with this conceit in mind. Remarkably, we find that many, although not all, features of the PDE model are recapitulated in the MES system and in comparable parameter ranges. In the MES we find stationary patterns and periodic orbits of both very short and very long periods (of > 300 time steps). On a short-time scale these long-period solutions can appear quite irregular and, to a degree, correspond to the spatio-temporal chaotic patterns of the PDE model. Of course, it is noted that similarly long investigations of the PDE model are restricted by their numerical feasibility and the very long-time behaviour of chaotic patterns in the PDE model would be worthy of further investigation. In [22] arguments were given that imply chaotic orbits exist for the PDE model and, while we have not yet observed chaotic orbits in the MES system, this is not overtly surprising given the simplifications in its formulation. As one example, while the positions of maxima are included in the MES, their shape is not: merging/emerging events in the PDE model do not obey the strict symmetric properties of the MES. Thus, we cannot expect a full recovery of the PDE behaviour and, while the inclusion of randomness (Section 4.5) allows random orbits, the MES loses its deterministic nature.

Another process excluded here is the spatial movement of spikes. In [13] it was shown that a single interior spike in the chemotaxis model without logistic growth is unstable to translational modes: an interior spike would move towards one of the boundaries. In the MES model this is equivalent to $l_m = \infty$, $l_a = \infty$ and each single interior spike is immediately absorbed into one of the boundaries. With logistic growth the chemotaxis model reveals movement of spikes towards one another prior to merging and, while this effect is certainly relevant in some cases, it does not appear to play a major role in the merging-emerging dynamics. The drift of spikes of order 1 is implicitly included into instantaneous merging (or absorption into the boundary), while translational instabilities of small order are neglected. Possible future extensions would be to consider more sophisticated (but deterministic) operations that impose asymmetric merging/emerging events, along with spike movement.

The MES system satisfactorily explains many of the pattern forming features of the logistic chemotaxis model and, hence, forms the basis of a caricature model for exploring dynamics in that system. Moreover, it represents a new class of discrete set-valued dynamical systems that should be studied in its own right. Here we have shown selected examples of its rich dynamical properties and further studies will enhance our understanding of pattern interactions.

Appendix A. **Alternative Merging and Emerging Operators.** In this appendix we summarise alternative emerging and merging operators. The base case
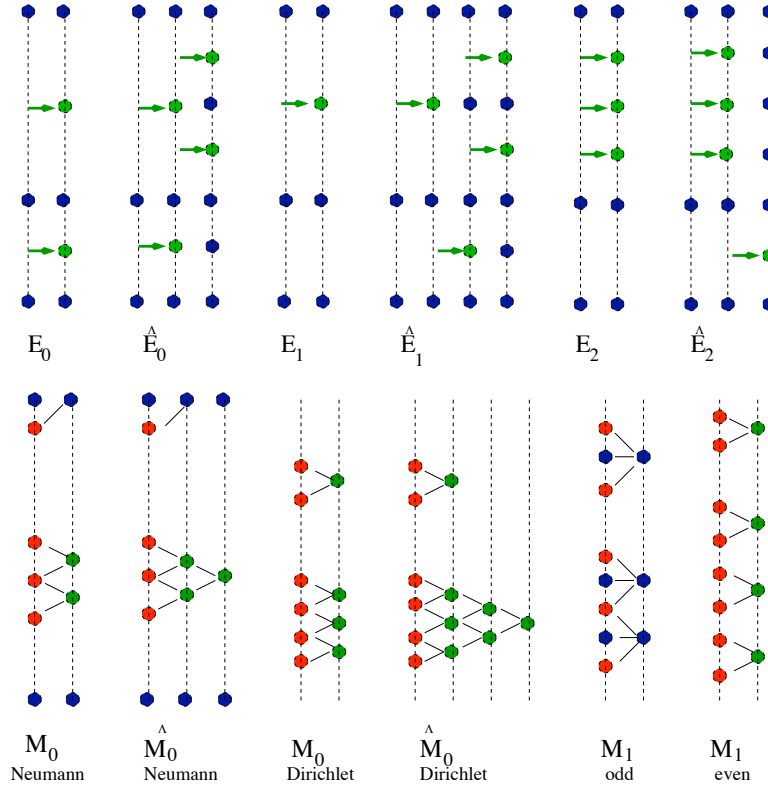
FIGURE 17. Schematic of (top row) emerging and (bottom row) merging operators. Blue points are unchanged by the iteration, green points emerge and red points vanish due to merging. Emerging is also indicated through a green arrow, while merging by short solid lines (color version online).

(M_0, E_0) is the easiest to formulate, however the final case considered, $(\hat{E}_2, \hat{M}_1)$, appears closest in behaviour to the PDE simulations and is used in the majority of the simulations. While the base case (E_0, M_0) was formally defined in section 2, we repeat it here for completeness. The following emerging and merging operators are illustrated in Figure 17.

Emerging Operators:
We assume $a \in \mathcal{P}$ and the emerging length $l_e > 0$ is given.

: **(i) Base case.** Let $J_e^0 := \{j : a_{j+1} - a_j > l_e\}$ denote the index set of all intervals longer than l_e (possibly empty). Then

$$E_0(a) := a + \sum_{J_e^0} \left\{ \frac{a_{j+1} + a_j}{2} \right\}.$$

: **(ii) Repeated base case.** An emerging event may still leave subintervals longer then l_e. Here we repeatedly apply E_0 until all intervals are shorter than l_e:

$$\hat{E}_0(a) := E_0 \circ E_0 \circ \cdots \circ E_0(a).$$

Note this is a finite iteration of E_0 until all intervals are shorter than l_e.

: **(iii) Emerge in the largest interval.** We let $J_e^1 := \{j : a_{j+1} - a_j = max\{a_l - a_{l-1}, l = 1, \ldots, n - 1\} > l_e, \}$ and let emergence only take place in the longest interval:

$$E_1(a) := a + \sum_{J_e^1} \left\{ \frac{a_{j+1} + a_j}{2} \right\}.$$

: **(iv) Repeated largest interval emergence.** E_1 is repeatedly applied until all possible emergence events have occurred:

$$\hat{E}_1(a) := E_1 \circ E_1 \circ \cdots \circ E_1(a).$$

Note that this infinite composition of E_1 terminates after a finite time, since the domain will continue to be filled until all intervals are shorter than l_e.

: **(v) Mega-emerging in large intervals.** If an interval is longer than > 1 multiples of l_e, we allow the addition of multiple points, equidistantly distributed and closer than l_e. We let $J_e^2 := \{j : a_{j+1} - a_j = \max\{a_l - a_{l-1}, l = 1 \ldots, n\} > l_e\}$, and estimate the number of additional emerging points as $\sigma := floor(\frac{a_{j+1} - a_j}{l_e})$. Then

$$E_2(a) := a + \sum_{J_e^2} \sum_{k=1}^{\sigma} \left\{ \frac{k}{\sigma + 1}(a_{j+1} - a_j) \right\}.$$

: **(vi) Repeat mega-emerging in large intervals.** As previously, we repeatedly apply E_2:

$$\hat{E}_2(a) := E_2 \circ E_2 \circ \cdots \circ E_2(a).$$

Again, the limit is a finite composition of E_2.

Merging operator for Neumann boundary conditions. For Neumann boundary conditions the PDE typically generates two fixed maxima at the boundary of the domain. This is reflected in a merging algorithm whereby merging near the boundary results in absorption into the boundary. Given $a \in \mathcal{P}$ and a merging length $l_m > 0$.

: **(i) Base case, Neumann.** We define two merging sets, for inner and boundary merging events: $J_m^0 := \{j : |a_{j+1} - a_j| < l_m, j = 2, \ldots, n - 1\}$; $\tilde{J}_m^0 := \{1 : a_1 < l_m/2\} \cup \{n - 1 : 1 - a_{n-1} < l_m/2\}$. Then the *merging operator* $M_0 : \mathcal{P} \to \mathcal{P}$ is defined as

$$M_0(a) := a - \sum_{\tilde{J}_m^0} \{a_j\} - \sum_{J_m^0} \{a_{j+1}, a_j\} + \sum_{J_m^0} \left\{ \frac{a_{j+1} + a_j}{2} \right\}.$$

: **(ii) Repeated base case.** A merging event can still lead to intervals shorter than l_m, hence we repeat the single merger until all intervals are longer than l_m:

$$\hat{M}_0(a) := M_0 \circ M_0 \circ \cdots \circ M_0(a).$$

As for emerging, this composition defines a finite number of iterations, terminating when all intervals are longer than l_m.

Merging operator for Dirichlet boundary conditions. For Dirichlet boundary conditions, boundary maxima are never observed in the chemotaxis model and we therefore assume no boundary mergers.

: (iii) Base case, Dirichlet. Let $J_m^0 := \{j : |a_{j+1} - a_j| < l_m\}$ denote the set of all critical intervals, then

$$M_0(a) := a - \sum_{J_m^0} \{a_{j+1}, a_j\} + \sum_{J_{m0}^D} \left\{ \frac{a_{j+1} + a_j}{2} \right\}.$$

: (iv) repeated base case:

$$\hat{M}_0(a) := M_0 \circ M_0 \circ \cdots \circ M_0(a).$$

Mega-merger for both, Neumann and Dirichlet conditions

: (v) mega-merger: It has been observed in the PDE, that multiple merging intervals that are side by side, lead to interaction of more than one maximum. For example, three local maxima can merge into one maximum (see Figures 1, 17 above). To reflect this behaviour, we define a mega-merger for even and for odd numbers of neighbouring merging intervals. Let

$$J_{\text{odd}}^1 := \{j : \exists k_{\text{odd}} \text{ odd} : a_{j+i} - a_{j+i-1} = min\{a_{l+1} - a_l\} \forall i = 1, \ldots, k\}$$

and

$$J_{\text{even}}^1 := \{j : \exists k_{\text{even}} \text{ even} : a_{j+i} - a_{j+i-1} = min\{a_{l+1} - a_l\} \forall i = 1, \ldots, k\}.$$

Then

$$
\begin{aligned}
M_1(a) \quad := \quad & a - \sum_{j \in J_{\text{even}}^1} \sum_{p=0,\text{even}}^{k_{\text{even}}} \{a_{j+p}\} \\
& - \sum_{j \in J_{\text{odd}}^1} \sum_{p=1}^{k_{\text{odd}}} \{a_{j+p}, a_j\} + \sum_{j \in J_{\text{odd}}^1} \sum_{p=1,\text{odd}}^{k_{\text{odd}}} \left\{ \frac{a_{j+p} + a_{j+p-1}}{2} \right\}.
\end{aligned}
$$

The action of the mega merger is illustrated in Figure 17.

: (vi) repeated mega-merger:

$$\hat{M}_1(a) := M_1 \circ M_1 \circ \cdots \circ M_1(a).$$

REFERENCES

[1] M. Aida, T. Tsujikawa, M. Efendiev, A.Yagi, and M. Mimura. Lower estimate of the attractor dimension for a chemotaxis growth system. *J. London Math. Soc.*, 74:453–474, 2006.

[2] V. Andasari, A. Gerisch, G. Lolas, A. South, and M.A.J. Chaplain. Mathematical modeling of cancer cell invasion of tissue: Biological insight from mathematical analysis and computational simulation. *J. Math. Biol.*, 63(1):141–172, 2011.

[3] S. Banerjee, A.P. Misra, and L. Rondoni. Spatiotemporal evolution in a (2+ 1)-dimensional chemotaxis model. *Physica A: Statistical Mechanics and its Applications*, 391:107–112, 2012.

[4] D. Barkley. Simplifying the complexity of pipe flow. *Physical Review E*, 84(1):016309, 2011.

[5] R. Baronas and R. Šimkus. Modelling the bacterial self-organization in circular container along the contact line as detected by bioluminescence imaging. *Nonlinear Anal. Model. Control*, 16:270–282.

[6] J.T. Bonner. *The social amoebae: the biology of cellular slime molds*. Princeton University Press, 2008.

[7] E.O. Budrene, H.C. Berg, et al. Complex patterns formed by motile cells of Escherichia coli. *Nature*, 349(6310):630, 1991.

[8] G. de Vries. Bursting as an emergent phenomenon in coupled chaotic maps. *Phys. Rev. E*, 64, 051914, 2001.

[9] Y. Dolak and T. Hillen. Cattaneo models for chemotaxis, numerical solution and pattern formation. *J. Math. Biol.*, 46(2):153–170, 2003.

[10] T. Hillen and K.J. Painter. A user's guide to PDE models for chemotaxis. *J. Math. Biol.*, 58:183–217, 2009.

[11] T. Hillen, K.J. Painter, and M. Winkler. Convergence of a cancer invasion model to a logistic chemotaxis model. *Math. Mod. Meth. Appl. Sci.*, 23(1):165–198, 2013.

[12] D. Horstmann. From 1970 until present: The Keller-Segel model in chemotaxis and its consequences I. *Jahresberichte der DMV*, 105(3):103–165, 2003.

[13] K. Kang, T. Kolokolnikov, M.J. Ward. The stability and dynamics of a spike in the one-dimensional Keller-Segel model. *IMA J. Appl. Math.*, 72:140-162, 2007.

[14] J.P. Keener. Chaotic Behavior in Piecewise Continuous Difference Equations. *Trans. AMS* 261: 589-604, 1980.

[15] E.F. Keller and L.A. Segel. Initiation of slime mold aggregation viewed as an instability. *J. Theo. Biol.*, 26:399–415, 1970.

[16] E.F. Keller and L.A. Segel. Model for chemotaxis. *J. Theor. Biol.*, 30:225–234, 1971.

[17] T. Kolokolnikov and J. Wei. Basic mechanisms driving complex spike dynamics in a chemotaxis model with logistic growth. submitted to Physica D, 2013.

[18] K. Kuto, K. Osaki, T. Sakurai, and T. Tsujikawa. Spatial pattern formation in a chemotaxis-diffusion-growth model. *Physica D: Nonlinear Phenomena*, 2012.

[19] H.G. Othmer and J. Dallon. Models of Dictyostelium aggregation. In W. Alt, A. Deutsch, and G. Dunn, editors, *Dynamics of Cell and Tissue Motion*. Birkhäuser, 1996.

[20] H.G. Othmer and C. Xue. Multiscale models of taxis-driven patterning in bacterial populations. *SIAM Appl. Math.*, 70(1):133–167, 2009.

[21] M.R. Owen and J.A. Sherratt. Pattern formation and spatiotemporal irregularity in a model for macrophage–tumour interactions. *J. Theor. Biol.*, 189:63–80, 1997.

[22] K.J. Painter and T. Hillen. Spatio-temporal chaos in a chemotaxis model. *Physica D*, 240:363–375, 2011.

[23] I.G. Pearce, M.A.J. Chaplain, P.G. Schofield, A.R.A. Anderson, and S.F. Hubbard. Chemotaxis-induced spatio-temporal heterogeneity in multi-species host-parasitoid systems. *J. Math. Biol.*, 55:365–388, 2007.

[24] R. Šimkus and R. Baronas. Metabolic self-organization of bioluminescent escherichia coli. *Luminescence*, 26:716–721, 2011.

[25] Z.A. Wang and T. Hillen. Pattern formation for a chemotaxis model with volume filling. *Chaos*, 17(3):13 pages, 2007.

[26] D.D. Woodward, R. Tyson, M.R. Myerscough, J.D. Murray, E. Budrene, and H.C. Berg. Spatio-temporal patterns generated by *Salmonella typhimurium*. *Biophys. J.*, 68:2181–2189, 1995.

E-mail address: thillen@ualberta.ca

E-mail address: jeffreyz@ualberta.ca

E-mail address: K.Painter@hw.ac.uk